Check for updates

AGU ADVANCING EARTH AND SPACE SCIENCES

Geophysical Research Letters®

RESEARCH LETTER
10.1029/2025GL121307

Key Points:

- The impact of stratosphere-troposphere interactions on tropical cyclone intensity is investigated in idealized simulations
- A modified potential intensity is introduced, that accounts for the upper-level warming in the outflow temperature
- Vertical advection near the tropopause is the main contributor to upper-level warming and reduced intensity, and is stronger with warmer SST

Supporting Information:

Supporting Information may be found in the online version of this article.

Correspondence to:

G. A. Charinti,
giousefalexandros.charinti@ista.ac.at

Citation:

Charinti, G. A., Davin, A., Polesello, A., Muller, C., & Pasquero, C. (2026). Impact of upper-level warming on tropical cyclone intensity. *Geophysical Research Letters*, *53*, e2025GL121307. https://doi.org/10.1029/2025GL121307

Received 22 DEC 2025
Accepted 14 AUG 2026

Impact of Upper-Level Warming on Tropical Cyclone Intensity

Giousef Alexandros Charinti[1], Andrea Davin[2], Andrea Polesello[1], Caroline Muller[1], and Claudia Pasquero[2]

[1]Institute of Science and Technology Austria, Klosterneuburg, Austria, [2]University of Milan-Bicocca, Milan, Italy

Abstract Deep convection from tropical cyclones (TCs) can reach the height of the tropopause and as such an interaction between the upper troposphere and lower stratosphere is likely to occur. Such interactions have been reported in both numerical and observational studies, mainly showing that subsidence from the stratosphere into the eye of an intensifying storm leads to a high-level warm core. However, the effect of this upper-level warming on the intensity of the TCs is not yet well understood. In this study, we show that subsiding air from the stratosphere beyond subsidence in the eye is the reason for the upper-level warming in idealized simulations. We further show that it is possible to quantify the effects of the upper-level warming on the potential intensity of the TC. Finally, we conclude that overshooting convection into the stratosphere causes the observed subsidence, as both become more pronounced with increasing sea-surface tempera tures (SST).

Plain Language Summary Developing clouds in a tropical cyclone (TC) can reach high altitudes in the atmosphere, sometimes crossing the boundary between the troposphere and the stratosphere. Previous studies have observed that warm stratospheric air can descend in the eye of an intensifying storm, leading to a high-level warm core. However, it is still not well understood what effect this upper-level warming has on the intensity of the storm itself. In this study, we show that stratospheric air can also descend in other areas of the cyclone beyond the eye. We further show that the observed upper-level warming can be factored in when computing a maximum potential intensity for the storm. Finally, we conclude that the deepest clouds in the cyclone that reach into the stratosphere are responsible for triggering the descent of stratospheric air, and both are stronger with increasing sea-surface temperatures (SST).

1. Introduction

Forecasts of tropical cyclone (TC) track and intensity have improved considerably in recent years (Cangialosi et al., 2020; Wang et al., 2023). Yet, predicting TC intensity remains a major scientific challenge, and progress has been relatively slow compared to TC track prediction, due to the numerous near-surface and upper-level processes involved (Rogers, 2021). As with any forecasting problem, a better understanding of the underlying physical processes is essential for improving tropical cyclone intensity prediction. From a theoretical point of view, the maximum potential intensity (PI) has been a widely used metric as an upper bound for tropical cyclone intensity based on the pre-storm environment (Emanuel, 1986, 2003). However, it is well known that in reality tropical cyclones rarely reach their PI (Emanuel, 2000; Gilford et al., 2019; Wing et al., 2007), even without landfall, due to several limiting factors, such as wind shear.

A common approach to understand the impact of these processes on TC intensity is the use of a modified version of PI. For instance, several studies have investigated the impact of sea-surface temperature (SST) cooling induced by upper-ocean mixing due to the TC passage (e.g., Balaguru et al., 2015; Hallam et al., 2021; Lin et al., 2013). They introduced a modified PI using the mean temperature of the ocean mixed layer instead of SST, to incorporate the effects of TC-induced upper-ocean mixing and SST cooling on TC intensification. This modified PI is found to be more indicative of peak TC intensity than the one based on pre-storm SST. Likewise, several studies have introduced a modified PI to account for vertical wind shear (e.g., Chavas et al., 2025; Pal & Chatterjee, 2022). More precisely, their modified PI accounts for the reduction of PI by vertical wind shear, based on empirical relationships that incorporate the potential impact of dry, low-entropy air advection into the TC by environmental vertical wind shear, for example, Tang and Emanuel (2012).

10.1029/2025GL121307

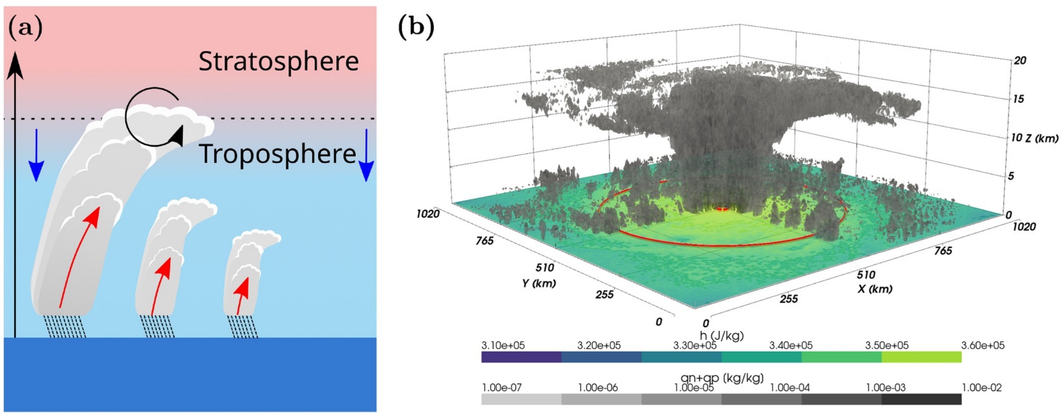

Figure 1. (a) Schematic of the mature cyclone showing how overshooting deep convection triggers an exchange between the upper troposphere and stratosphere, separated by the tropopause (dotted line). (b) Simulation output with an SST of 300 K at day 20 showing clouds (isosurfaces of $q_n + q_p$ non precipitating and precipitating mixing ratios respectively) and surface moist static energy. Red lines show the inner and outer boundaries of the area of interest at the surface defined by angular momentum surfaces at r_i and r_o respectively. Clouds are removed in the front quadrant and the z-axis is stretched by a factor 20 for better visualization.

Beyond the mechanisms mentioned above, upper-level processes beyond wind shear may also play a role, though they have received comparatively less attention. For instance, Zhang and Chen (2012) showed that, in an idealized simulation of Hurricane Wilma, convective bursts in the eyewall induced stratospheric air descent into the eye. This led to the formation of a high-level warm core early in the TC's life cycle. Similarly, Ohno and Satoh (2015) used numerical experiments to demonstrate that upper-level warming can also result from convective bursts during the mature stage. In another numerical study, Kieu et al. (2016) proposed a new mechanism, in which an inflow layer in the low stratosphere enhances warm core formation and, in turn, increases the intensity of the TC (by lowering surface pressure). However, more recently, Polesello et al. (2025) showed in idealized simulations that deep convection interacting with the stratosphere can instead increase upper-level stability and weaken the storm (Figure 1a).

TC interactions with the stratosphere have also been reported in observational studies. Rodgers et al. (1990) showed how the upper tropospheric ozone distribution can be affected by the passage of TCs. From their observations, they concluded that stratospheric interaction is more pronounced in intensifying TCs and can lead to dry air intrusion in the eye. This intrusion ultimately weakens convection in the eyewall and thus the TC intensity, consistent with the aforementioned numerical study. In a more recent study, Roy et al. (2023) verified that TCs over the Indian ocean interact with the stratosphere by analyzing ozone spatial anomalies associated with their passage.

Our goal here is to investigate these upper-level processes in detail, and assess their impact on TC intensity. To isolate the effects of upper-level processes, we employ idealized simulations with constant SST (in space and time) (Figure 1b) and no large-scale environmental shear. More precisely, we address the following questions:

- How do interactions between the troposphere and the stratosphere reduce the peak intensity of the cyclones?
- Can this effect be captured in a physics-based modified PI?
- Can we clarify the physical processes involved and their sensitivity to SST?

We show that an interaction of the cyclone with the stratosphere and a subsequent warming of the upper troposphere is the key reason why our simulated TCs are weaker than the PI theory would predict, consistent with Polesello et al. (2025). We further explore this by introducing a modified PI that accounts for the upper-level warming in the outflow temperature. Finally, we show that vertical advection between the stratosphere and the upper troposphere is the main contributor to upper-level warming using an energy budget analysis. Furthermore, we show that vertical advection becomes stronger with higher SSTs.

2. Methods

2.1. Cloud-Resolving Model

In this work, we use the Cloud-Resolving Model (CRM) System for Atmosphere Modeling (SAM), version 6.10.8 (Khairoutdinov & Randall, 2003). The model runs in the idealized setting of radiative-convective equilibrium (RCE), characterized by an energy balance between surface fluxes and atmospheric radiative cooling. Moist convection conserves frozen moist static energy (MSE) denoted h (Wing & Emanuel, 2014):

$$h = c_p T + gz + L_v q_v - L_f q_{\mathrm{ice}}, \tag{1}$$

where T denotes temperature, z height, q_v water vapor mixing ratio, q_{ice} mixing ratio of all ice phases, g gravitational acceleration, c_p heat capacity of dry air and L_v, L_f latent heat of vaporization and fusion respectively (see Section S1 in Supporting Information S1 for details).

2.2. Simulations Setup

Our simulations are run in a doubly periodic horizontal 1,024 km × 1,024 km domain with a 4 km horizontal resolution. The domain spans 64 levels in the vertical direction, between 37.5 m and 27 km. The top of the domain includes a sponge layer, extending from 18 to 27 km, where winds are relaxed to 0 such that gravity waves are damped. The vertical grid is not regular and is finer at the bottom starting at a resolution of 80 m, and coarser in the mid-troposphere (around 500 m). We employ an f-plane with a Coriolis parameter of $f = 10^{-4}$ s^{-1}, which is stronger than typical tropical values. This choice reduces the radial extent of tropical cyclones, allowing for a smaller computational domain and lower computational cost (Muller & Romps, 2018). No diurnal cycle is considered and the solar radiation intensity is fixed at 413 Wm^{-2}, similar to Shamekh et al. (2020); Polesello et al. (2025). We note that we conducted a run with an SST of 300 K and a diurnal cycle, where the daily mean solar radiation is equal to the above, and we did not notice any significant changes in the daily mean results.

We conduct five sets of simulations, each with a prescribed constant SST of 294 K, 297 K, 300 K, 303 K, or 306 K (initialized with mean profiles from small-domain simulations with the corresponding SST, Section S2 in Supporting Information S1). For each SST, we run three ensemble members, differing only in the random seed used for the initial perturbations. Although this ensemble size is relatively small, it reflects a compromise between computational cost and the need to represent variability in the results.

2.3. Analysis: Identifying Convective Regions

In this study, we focus on troposphere–stratosphere heat exchanges resulting from convection in the eyewall and spiraling bands. To do so, we first need to define the convective regions within the tropical cyclone. In tropical cyclones, convection develops on slanted surfaces of constant angular momentum,

$$M = r u_t + \frac{1}{2} f r^2, \tag{2}$$

where r is the radius from the eye, and u_t the tangential velocity. The center of the TC is located following Hodges et al. (2017). In order to exclude effects from subsidence in the eye, we compute radial averages starting from a surface radius $r_i = 10$ km and then follow a surface of constant angular momentum in height. As not the whole domain is relevant for the upper level warming which we aim to quantify, at each timestep we set an outer bound r_o at the radius where the surface MSE (h at $z = 0$) drops to its instantaneous 75th percentile. This value is chosen because it encloses the area where most of the slantwise convection occurs throughout the simulation (including the eyewall and spiraling bands). Figure 1b shows the area bounded by r_i and r_o at the surface at day 20 of one of the 300 K SST simulations. We note that r_o is not constant in time, and its evolution is shown in Figure S1a in Supporting Information S1. All results based on r_0 are robust, as long as the surface MSE percentiles on the radius threshold lie between 50% and 90%.

In our analysis, we define the depth of convection by identifying the equilibrium level using MSE as a diagnostic variable, since MSE is conserved in moist convection. Convection transports air parcels with MSE from the surface upward, and therefore can only produce MSE values in the free troposphere that are equal to, or lower than, those at the surface. Any higher MSE values must arise from processes other than convection. Accordingly, we define the equilibrium level, EL_h, as the height in the upper troposphere where MSE first exceeds its surface value, that is,

$$\mathrm{EL}_h(r) = z\big(\overline{h}(r,z) > \overline{h}(r,z=0)\big), \tag{3}$$

where overline denotes azimuthal average, and this process is repeated at each r, starting from $\overline{h}(r,z = 0)$ and then detecting EL_h following surfaces of constant angular momentum in height. By this definition, the region above EL_h can only be influenced either by overshooting convection or by non-convective processes, such as radiative effects or the descent of warm stratospheric air.

3. Results

3.1. Overview of Upper-Level Warming

First, as a means of showing the upper-level warming in time, Figure 2a shows a Hovmöller plot of the vertical profile of MSE. MSE is averaged in the convective region, that is, between the angular momentum surfaces starting at r_i and r_o, and over simulations with an SST = 300 K. Here and in the following, all simulations are time-shifted so that $t_{\max} = 10\,\mathrm{d}$ for easier comparison.

Before $t_{\max}$, convection is weak and disorganized, and both boundary-layer and upper-level MSE remain low. As the cyclone develops (days 7–8), convection organizes and column-mean MSE increases, followed by a slight rise in EL_h. Near $t_{\max}$, upper-level MSE exceeds boundary-layer MSE, indicating that convection alone does not explain the increase. Consistent with this upper-level warming and greater stability, EL_h decreases after $t_{\max}$ and remains low until about day 20, when MSE gradually returns to pre-cyclone values.

Since post-$t_{\max}$ decay was addressed in Polesello et al. (2025), we focus here instead on the period around $t_{\max}$ to quantify upper-level warming impact on peak intensity and troposphere–stratosphere interactions.

3.2. Modified Potential Intensity

Our goal here is to estimate the impact of upper-level warming on the TC peak intensity. To that end, we introduce the maximum potential velocity V_p as first formulated by Emanuel (1986) and later adapted by Emanuel (2003) and others, to

$$V_p^2 = \frac{c_k}{c_d}\frac{T_s - T_0}{T_s}\big(k_s^* - k_1\big), \tag{4}$$

where T_s and T_0 are the surface (SST) and outflow temperature respectively, k_s^* and k_1 the enthalpy at the surface and first model level respectively, defined as

$$k = c_p T + L_v q_v, \tag{5}$$

and $*$ denotes saturation. As dissipative heating does not occur in SAM (Cronin & Chavas, 2019), we do not apply the denominator correction of Bister and Emanuel (1998). V_p is usually evaluated from pre-storm conditions, such that it essentially shows the maximum potential velocity that a cyclone can reach based on the thermodynamic environment prior to its genesis.

As the cyclone forms and intensifies, it impacts its environment. In particular, we expect the upper-level warming to affect the outflow temperature, and thus the Carnot efficiency (second factor on the right-hand side of Equation 4). We thus modify PI to account for the upper-level warming by letting the outflow temperature evolve in time

$$V_p^2(t) = \frac{c_k}{c_d}\frac{T_s - T_0(t)}{T_s}\big(k_s^* - k_1\big), \tag{6}$$

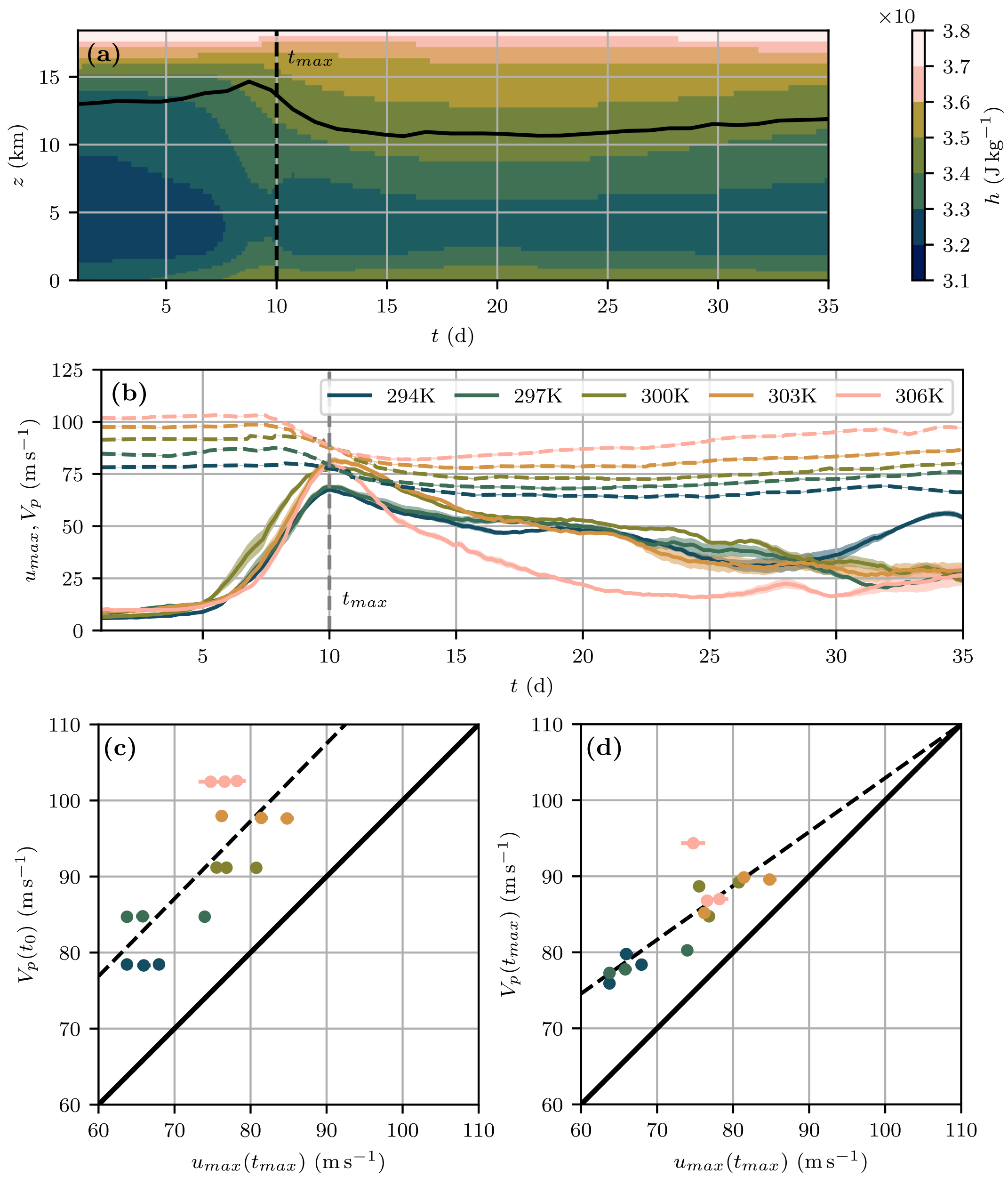

Figure 2. (a) Hovmöller plot of h within r_i and r_o for SST = 300 K, with the solid line indicating EL_h and the dashed line $t_{\max}$. (b) Maximum observed tangential velocity $u_{\max}$ (solid) and modified PI V_p (dashed) colored by each SST, with the shading indicating the 95% confidence interval of the mean across each SST ensemble. (c) Scatter plot of $u_{\max}(t_{\max})$ versus $V_p(t_0)$ showing all simulations, colored by SST, with errorbars indicating 95% confidence interval of the mean across 3 timesteps around $t_{\max}$. The dashed and solid lines show the regression line and $y = x$ respectively. (d) As in (c) but V_p is evaluated around $t_{\max}$.

where all terms are evaluated at the first time step, except T_0 which evolves in time, averaged at $z = \mathrm{EL}_h \pm 1$ km. As before, all terms are averaged in the convective region, that is, between radii r_i and r_o.

Figure 2b shows the maximum observed tangential velocity $u_{\max}$ (solid) and the modified PI (dashed) as a function of time. At day 0 of the graph, no cyclone exists in any of the simulations, and thus the modified PI value is equal to the PI of the pre-storm environment (the outflow temperature does not change significantly between the beginning of the simulation and day 0, which corresponds here to 10 days before $t_{\max}$). The outflow temperature increases a few days before $t_{\max}$ which leads to a drop in PI (Figure 2b). The drop typically occurs earlier for warmer SST, and for the coldest SST, 294 K, this drop occurs at $t_{\max}$. The warming of the upper troposphere results in a lowering of EL_h (Figure S1b in Supporting Information S1). Overall, our results confirm that PI is never reached in the simulations. Furthermore, our modified PI, accounting for upper-level warming around $t_{\max}$, better matches the actual TC peak intensity.

This can be further quantified by comparing the maximum velocity in each simulation, $u_{\max}$, averaged between 1 day before and after $t_{\max}$, and its corresponding pre-storm PI evaluated at the first timestep of each simulation, $V_p(t_0)$ (Figure 2c). PI is higher at warmer SST and is indeed always larger than the actual velocity maximum. However, when we evaluate the modified PI around $t_{\max}$ (following the same time averaging procedure as $u_{\max}$) in Figure 2d, we see that the modified PI drops and approaches the actual TC intensity. We also find that higher SSTs lead to a larger drop in PI, whereas the lowest SST at 294 K barely shows any drop at all. An intuitive way to interpret this result would be a larger warming of T_0 with higher SST since this would result in a larger PI drop, which is indeed the case around $t_{\max}$ (Figure S1c in Supporting Information S1). Eventually, once the cyclone is formed, T_0 plateaus around 230 K in all simulations. Therefore, it is the warming of the upper troposphere around $t_{\max}$ which is relevant for the intensity drop, and the warming occurs faster at warmer SST. This raises the question as to which mechanism affects the upper-level heating rate, which we address in the following sections (note that the upper troposphere temperature increases in all simulations, Figure S2 in Supporting Information S1).

3.3. Quantifying Troposphere-Stratosphere MSE Exchange

Our qualitative evidence for troposphere-stratosphere exchanges came from the observation that upper-level MSE increases beyond that expected from convection (Section 3.1). Here our goal is to quantitatively investigate these exchanges and the associated upper-level warming. Note that we use MSE increase and upper-level warming interchangeably, since MSE changes at these upper-tropospheric heights are largely dominated by temperature changes. To that end, we analyze the budget of MSE near the equilibrium level, which we can write as

$$\frac{\partial \rho h}{\partial t} + \nabla \cdot (\rho \boldsymbol{u} h) = \text{Diabatic terms}, \tag{7}$$

where ρ and $\boldsymbol{u}$ are the density and the wind velocity respectively. Diabatic heating in the upper troposphere can be mainly attributed to radiation, which is expected to be much smaller than the advective term in the convective regions of interest (as will be confirmed in the next section and Figure S5a in Supporting Information S1). Thus, by neglecting the diabatic terms on the right-hand side of Equation 7 we can write

$$\frac{\partial \rho h}{\partial t} \approx \underbrace{-\nabla \cdot (\rho \boldsymbol{u} h)}_{\text{ADV}}, \tag{8}$$

where ADV indicates the advection of h. Equation 8 expresses the temporal change of h solely due to its advection.

We further decompose ADV into azimuthal mean and eddy components, by decomposing each variable $x = \bar{x} + x'$ into azimuthal mean $\bar{x}$ and departure from it x' (eddy term) similarly to Ohno and Satoh (2015) and Kieu et al. (2016). This results in a mean and eddy advection which we can write as

$$\overline{\text{ADV}} = \underbrace{-\rho \overline{u_r} \frac{\partial \overline{h}}{\partial r} - \rho \overline{w} \frac{\partial \overline{h}}{\partial z}}_{\text{Mean flow}} \underbrace{- \overline{\rho u_r' \frac{\partial h'}{\partial r}} - \rho \overline{\frac{u_\phi'}{r} \frac{\partial h'}{\partial \phi}} - \overline{\rho w' \frac{\partial h'}{\partial z}}}_{\text{Eddy flow}}, \tag{9}$$

where u_r, u_ϕ, w are the radial, tangential and vertical velocities, respectively (the exact derivation is shown in Section S4 in Supporting Information S1).

Figures 3a–3c show the azimuthal means of the total, mean and eddy vertical heat flux near EL_h in the 300 K simulations (other SSTs yield similar results, not shown).

We focus here on the vertical advection term, as it is the dominant term of the MSE increase (Figures 3d and 3e). We also focus (as before) on convective regions in the eyewall and spiraling bands, but outside the eye, since these

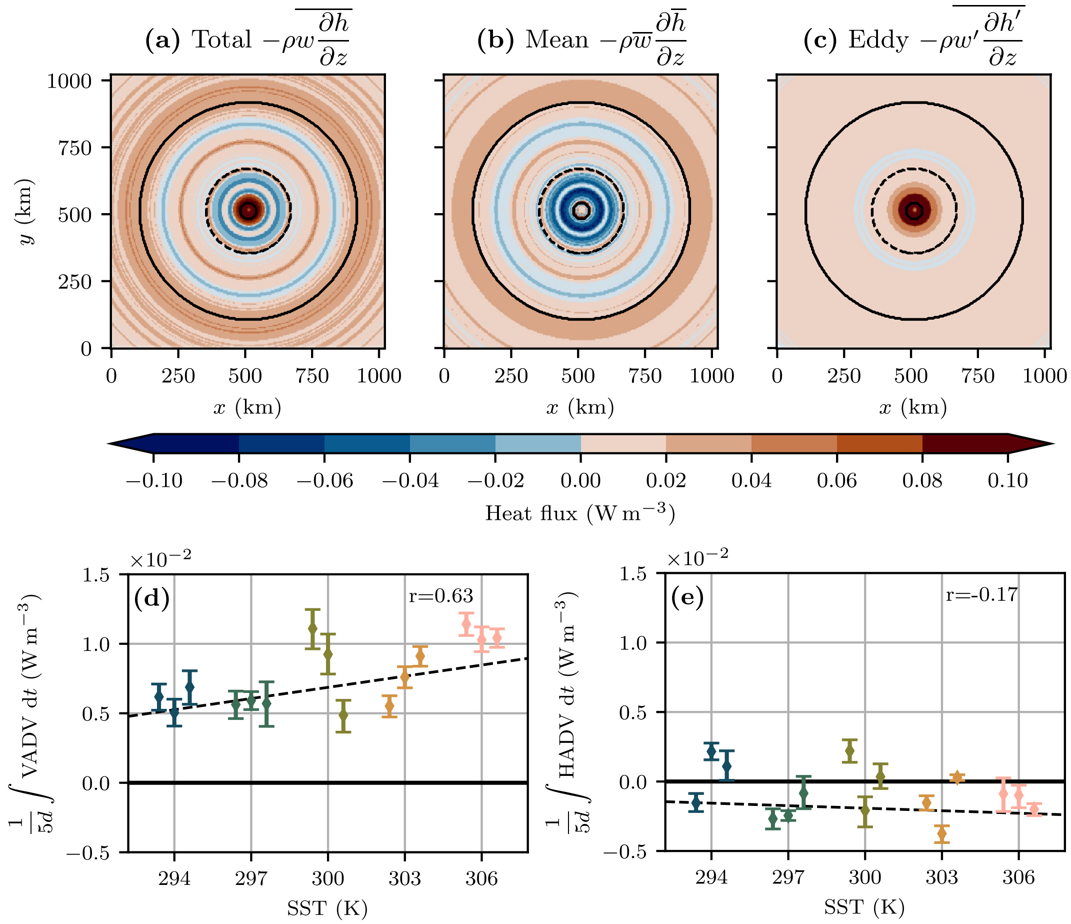

Figure 3. (a–c) Horizontal plot of total, mean and eddy vertical components in Equation 9 averaged over $t = t_{\max} \pm 1$ d, $z = \mathrm{EL}_h \pm 1$ km, $r_i \leq r \leq r_o$ and ensemble members with 300 K SST. The solid black lines indicate r_i, r_o and the dashed line the radius of the outer eyewall, all shown at EL_h. The colorbar is saturated to improve visualization. (d–e) Scatter plots of total (mean + eddy) vertical and horizontal advection terms respectively, averaged over the same heights as the above plots and radii, colored by their respective SST. The three ensemble members for each SST are shown at slightly different SST for visualization purposes. Advection terms are averaged from $t_{\max} - 3$ d to $t_{\max} + 1$ d, following the time window of the upper level warming before and around $t_{\max}$ (Figure S1c in Supporting Information S1). The error bars indicate 95% confidence interval of the mean in time and space, the dashed line the linear regression and r the correlation coefficient between the shown variable and SST. The latter two are computed by taking into account error bars.

are the regions where the upper-level warming is in our opinion relevant to the weakened convection and reduced TC intensity.

The overall warming from vertical advection (Figures 3a and 3d) is contributed by both mean and eddy terms (Figures 3b and 3c). The mean contribution has positive and negative regions. Since $\partial\overline{h}/\partial z > 0$ at EL_h (Figure S3 in Supporting Information S1), the sign of the mean contribution reflects the sign of $\overline{w}$. A positive sign implies that the domain is heating due to descending motion which brings warmer air from the stratosphere to lower levels. Conversely, upward motion in the eyewall and spiraling bands (Figure S3 in Supporting Information S1) yields a negative mean advection contribution. The rest of the domain warms due to compensating subsidence outside convection.

Although w' is larger in magnitude than $\overline{w}$ in general (Figure S3 in Supporting Information S1), $\partial h'/dz$ is much smaller than its mean counterpart, so that mean advection is an important contribution (especially at warm SST, Figure 3d). Only near the eyewall is the eddy contribution large and positive. This is because convection tends to advect anomalously high tropospheric MSE upward ($w' > 0, \partial h'/dz < 0$), yielding a positive eddy term. So the picture that emerges is that strong vertical velocities in updrafts do not contribute significantly to the upper-level

10.1029/2025GL121307

warming, since $\partial h'/dz$ is small, but they trigger compensating subsidence that, combined with the mean stratification, increases upper-level MSE, stability, and weakens the TC intensity.

We note in passing that Ohno and Satoh (2015), performed a similar budget analysis and concluded that the mean total advection is highest in the eye due to subsidence from the stratosphere. Our results suggest that the eddy term is instead more relevant in the eye and around the eyewall, and that the mean subsidence outside of the eyewall and the rainbands dominates the upper-level warming. In fact, we find that subsidence warming in the eye contributes to a slight intensification around $t_{\max}$ (not shown), consistent with, for example, Zhang and Chen (2012), but is eventually offset by outer-domain warming.

In the next section, we assess the impact of this upper-level MSE advection on the outflow temperature, which is relevant for TC intensity, and its sensitivity to SST.

3.4. Impact on Outflow Temperature and Sensitivity to SST

From the energy budget in the previous section, we can estimate the expected upper-level warming if we integrate the MSE flux in time from the moment the TC starts intensifying. The flux is integrated in time and averaged in space over the same domain as in the previous sections ($z = \mathrm{EL}_h \pm 1$ km and $r_i \le r \le r_o$) following

$$\Delta T_{\mathrm{ADV}} = \left\langle \frac{1}{\rho c_p} \int_{t_{\max}-3\mathrm{d}}^{t_{\max}+1\mathrm{d}} \mathrm{ADV}(r,z,t)\, dt \right\rangle, \tag{10}$$

where the brackets symbolize spatial averaging, and as in Figure 3 we start the time integration 3 days prior to $t_{\max}$ since this is when the upper level warming is triggered (Figure S1c in Supporting Information S1).

The warming estimated from MSE advection captures well the observed warming (Figure 4a). It is dominated by vertical advection (Figure 4b), consistent with the aforementioned small horizontal advection and radiation contributions (Figure 3 and Figure S5 in Supporting Information S1).

Both mean and eddy advection contribute to the warming (Figures 4c and 4d), but the mean contribution dominates the sensitivity to SST.

As noted in Figure 3, a large part of the warming comes from compensating subsidence outside convection. We thus hypothesize that the sensitivity to SST comes from more overshooting updrafts with warmer SST, which do not contribute directly to the warming (due to the smallness of $\partial h'/\partial z$), but contribute indirectly by triggering mean compensating subsidence and advection of low-stratospheric air. This is consistent with theory which predicts stronger convection with warmer SST (e.g., Singh & O'Gorman, 2013).

To estimate the intensity of convection, we compute the convective mass flux near the tropopause height z_T at the time of warming ($t_{\max} - 3$ d, $t_{\max} + 1$ d) defined by Williams and Jeevanjee (2025) as

$$M_{c,z_T} = \rho w_{\mathrm{up}} \sigma_{\mathrm{up}}, \tag{11}$$

here w_{up} is the mean upward velocity in convective regions with $w > 1\mathrm{ms}^{-1}$ and $q_n + q_p > 1 \times 10^{-5}$ kg kg^{-1}, and σ_{up} the fraction of the domain where convection occurs.

The mass flux from overshooting updrafts indeed increases with SST (Figure 4e). Furthermore, this increase is attributed to σ_{up} (Figure 4f), which dominates despite a slight decrease of ρw_{up} with SST (Figure S6 in Supporting Information S1).

This analysis supports our interpretation that upper-level warming is primarily driven by more overshooting updrafts, which trigger warming from compensating subsidence. We further show in Figure S7 in Supporting Information S1 that the time series of M_{c,z_T} and the subsiding mass flux ρw^- are well anti-correlated and in phase. As discussed earlier, we interpret this enhanced subsidence as resulting from overshooting updrafts, which strengthen troposphere–stratosphere interactions and promote upper-level warming, thereby causing a more rapid weakening of the TC at higher SSTs.

10.1029/2025GL121307

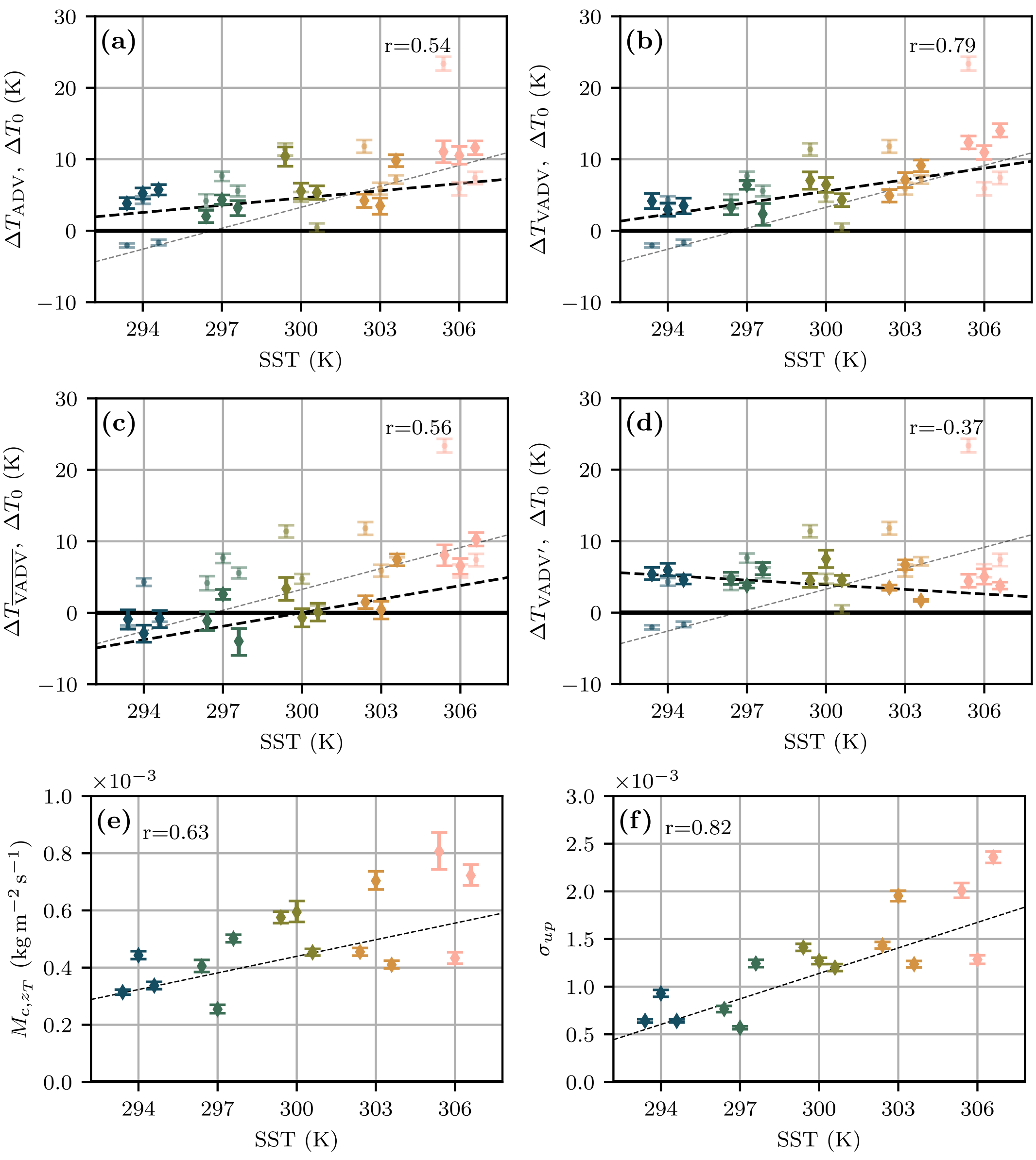

Figure 4. (a–d) Same as Figures 3d and 3e but showing warming due to total, vertical, vertical mean and vertical eddy advection (opaque). On all panels, the observed upper tropospheric warming ΔT_0 is repeated (transparent) for comparison. (e–f) Same as Figures 3d and 3e but showing convective mass flux near the tropopause M_{c,z_T} and convective fraction σ_{up} respectively.

4. Discussion

In this study, we identified an upper-level warming feedback which is caused when a TC intensifies in idealized simulations with different SSTs. We show that this feedback is the outcome of overshooting convection piercing into the stratosphere, which induces the descent of warm stratospheric air into the upper troposphere. The associated upper-level warming increases stability and weakens convection, thus limiting the TC intensity.

The impact of the warming can be quantified in a modified version of PI, which accounts for the warmer outflow temperature in the Carnot efficiency. In our analysis, we find that all simulations have a similar outflow temperature before the cyclone forms and after its peak intensity independent of their SST. However, the upper-level warming rate varies with SST, with higher SSTs producing faster warming.

In order to further investigate what affects the upper-level heating rate, we used the MSE budget near the equilibrium level. The upper-level warming estimated from MSE advection captures well the actual observed upper-level warming. Importantly, it captures its sensitivity to SST. We also find that the biggest contribution to the SST sensitivity originates from subsiding air (vertical advection of high-MSE stratospheric air).

A further decomposition of the heating rate into mean and eddy components shows that most of the SST sensitivity can be explained by the mean component. The enhanced mean subsidence and upper-level warming at higher SSTs is a consequence of overshooting updrafts, which cover a larger area with increasing SST, intensifying troposphere–stratosphere interactions through compensating subsidence of warm stratospheric air. This stronger circulation raises upper-tropospheric temperatures and stability, providing a negative feedback on convection and the TC.

As a result, TCs intensify with SST but not as fast as PI would suggest. Thus, this upper-level feedback may partially offset the rise of PI and limit TC intensity in warmer climates. More work is desirable to investigate whether similar processes occur in more realistic simulations and in observations, and to quantify its impact on TC intensity relative to other processes.

Conflict of Interest

The authors declare no conflicts of interest relevant to this study.

Availability Statement

The post-processed simulation data and the analysis scripts are available on Figshare https://doi.org/10.6084/m9.figshare.30933764 (Charinti et al., 2025).

Acknowledgments

GAC and CM acknowledge funding from the European Research Council (ERC) under the European Union's Horizon 2020 research and innovation program (Project CLUSTER, Grant Agreement No. 805041). AD and CP acknowledge support by the National Recovery and Resilience Plan project TeRABIT (Terabit network for Research and Academic Big data in Italy—IR0000022—PNRR Missione 4, Componente 2, Investimento 3.1 CUP I53C21000370006) in the frame of the European Union - NextGenerationEU funding. Open Access funding provided by Institute of Science and Technology Austria/KEMÖ.

References

Balaguru, K., Foltz, G. R., Leung, L. R., Asaro, E. D., Emanuel, K. A., Liu, H., & Zedler, S. E. (2015). Dynamic potential intensity: An improved representation of the ocean's impact on tropical cyclones. *Geophysical Research Letters*, *42*(16), 6739–6746. https://doi.org/10.1002/2015GL064822

Bister, M., & Emanuel, K. A. (1998). Dissipative heating and hurricane intensity. *Meteorology and Atmospheric Physics*, *65*(3–4), 233–240. https://doi.org/10.1007/BF01030791

Cangialosi, J. P., Blake, E., DeMaria, M., Penny, A., Latto, A., Rappaport, E., & Tallapragada, V. (2020). Recent progress in tropical cyclone intensity forecasting at the national hurricane center. *Weather and Forecasting*, *35*(5), 1913–1922. https://doi.org/10.1175/waf-d-20-0059.1

Charinti, G. A., Davin, A., Polesello, A., Muller, C., & Pasquero, C. (2025). NETCDF files and code scripts for impact of upper-level warming on tropical cyclone intensity. https://doi.org/10.6084/m9.figshare.30933764

Chavas, D. R., Camargo, S. J., & Tippett, M. K. (2025). Tropical cyclone genesis potential using a ventilated potential intensity. *Journal of Climate*, *38*(7), 1667–1689. https://doi.org/10.1175/JCLI-D-24-0186.1

Cronin, T. W., & Chavas, D. R. (2019). Dry and semidry tropical cyclones. *Journal of the Atmospheric Sciences*, *2019*(1), 1–20. https://doi.org/10.1175/JAS-D-18-0357.1

Emanuel, K. (2000). A statistical analysis of tropical cyclone intensity. *Monthly Weather Review*, *128*(4), 1139–1152. https://doi.org/10.1175/1520-0493(2000)128⟨1139:ASAOTC⟩2.0.CO;2

Emanuel, K. (2003). Tropical cyclones. *Annual Review of Earth and Planetary Sciences*, *31*(1), 75–104. https://doi.org/10.1146/annurev.earth.31.100901.141259

Emanuel, K. A. (1986). An air-sea interaction theory for tropical cyclones. Part I: Steady-state maintenance. *Journal of the Atmospheric Sciences*, *43*(6), 585–605. https://doi.org/10.1175/1520-0469(1986)043⟨0585:AASITF⟩2.0.CO;2

Gilford, D. M., Solomon, S., & Emanuel, K. A. (2019). Seasonal cycles of along-track tropical cyclone maximum intensity. *Monthly Weather Review*, *147*(7), 2417–2432. https://doi.org/10.1175/mwr-d-19-0021.1

Hallam, S., Guishard, M., Josey, S. A., Hyder, P., & Hirschi, J. (2021). Increasing tropical cyclone intensity and potential intensity in the subtropical Atlantic around Bermuda from an ocean heat content perspective 1955–2019. *Environmental Research Letters*, *16*(3), 034–052. https://doi.org/10.1088/1748-9326/abe493

Hodges, K., Cobb, A., & Vidale, P. L. (2017). How well are tropical cyclones represented in reanalysis datasets? *Journal of Climate*, *30*(14), 5243–5264. https://doi.org/10.1175/jcli-d-16-0557.1

Khairoutdinov, M. F., & Randall, D. A. (2003). Cloud resolving modeling of the ARM summer 1997 IOP: Model formulation, results, uncertainties, and sensitivities. *Journal of the Atmospheric Sciences*, *60*(4), 607–625. https://doi.org/10.1175/1520-0469(2003)060⟨0607:CRMOTA⟩2.0.CO;2

Kieu, C., Tallapragada, V., Zhang, D.-L., & Moon, Z. (2016). On the development of double warm-core structures in intense tropical cyclones. *Journal of the Atmospheric Sciences*, *73*(11), 4487–4506. https://doi.org/10.1175/JAS-D-16-0015.1

Lin, I.-I., Black, P., Price, J. F., Yang, C.-Y., Chen, S. S., Lien, C.-C., et al. (2013). An ocean coupling potential intensity index for tropical cyclones. *Geophysical Research Letters*, *40*(9), 1878–1882. https://doi.org/10.1002/grl.50091

Muller, C. J., & Romps, D. M. (2018). Acceleration of tropical cyclogenesis by self-aggregation feedbacks. *Proceedings of the National Academy of Sciences*, *115*(12), 2930–2935. https://doi.org/10.1073/pnas.1719967115

Ohno, T., & Satoh, M. (2015). On the warm core of a tropical cyclone formed near the tropopause. *Journal of the Atmospheric Sciences*, *72*(2), 551–571. https://doi.org/10.1175/JAS-D-14-0078.1

10.1029/2025GL121307

Pal, A., & Chatterjee, S. (2022). Influence of vertical wind shear on the maximum potential intensity of tropical cyclones over the Bay of Bengal region. *Journal of Earth System Science*, *131*(4), 255. https://doi.org/10.1007/s12040-022-02003-y

Polesello, A., Charinti, G. A., Meroni, A. N., Muller, C. J., & Pasquero, C. (2025). Intensity oscillations of tropical cyclones: Surface versus mid and upper tropospheric processes. *Journal of Advances in Modeling Earth Systems*, *17*(4), e2024MS004. https://doi.org/10.1029/2024MS004613

Rodgers, E. B., Stout, J., Steranka, J., & Chang, S. (1990). Tropical cyclone-upper atmospheric interaction as inferred from satellite total ozone observations. *Journal of Applied Meteorology*, *29*(9), 934–954. https://doi.org/10.1175/1520-0450(1990)029⟨0934:TCUAIA⟩2.0.CO;2

Rogers, R. F. (2021). Recent advances in our understanding of tropical cyclone intensity change processes from airborne observations. *Atmosphere*, *12*(5), 650. https://doi.org/10.3390/atmos12050650

Roy, C., Ravishankara, A. R., Newman, P. A., David, L. M., Fadnavis, S., Rathod, S. D., et al. (2023). Estimation of stratospheric intrusions during Indian cyclones. *Journal of Geophysical Research: Atmospheres*, *128*(3), e2022JD037. https://doi.org/10.1029/2022JD037519

Shamekh, S., Muller, C., Duvel, J.-P., & D'Andrea, F. (2020). Self-aggregation of convective clouds with interactive sea surface temperature. *Journal of Advances in Modeling Earth Systems*, *12*(11), e2020MS002. https://doi.org/10.1029/2020MS002164

Singh, M. S., & O'Gorman, P. A. (2013). Influence of entrainment on the thermal stratification in simulations of radiative-convective equilibrium. *Geophysical Research Letters*, *40*(16), 4398–4403. https://doi.org/10.1002/grl.50796

Tang, B., & Emanuel, K. (2012). A ventilation index for tropical cyclones. *Bulletin of the American Meteorological Society*, *93*(12), 1901–1912. https://doi.org/10.1175/BAMS-D-11-00165.1

Wang, W., Zhang, Z., Cangialosi, J. P., Brennan, M., Cowan, L., Clegg, P., et al. (2023). A review of recent advances (2018–2021) on tropical cyclone intensity change from operational perspectives, part 2: Forecasts by operational centers. *Tropical Cyclone Research and Review*, *12*(1), 50–63. https://doi.org/10.1016/j.tcrr.2023.05.003

Williams, A. I. L., & Jeevanjee, N. (2025). A robust constraint on the response of convective mass fluxes to warming. *Journal of Advances in Modeling Earth Systems*, *17*(4), e2024MS004. https://doi.org/10.1029/2024MS004695

Wing, A. A., & Emanuel, K. A. (2014). Physical mechanisms controlling self-aggregation of convection in idealized numerical modeling simulations. *Journal of Advances in Modeling Earth Systems*, *6*(1), 59–74. https://doi.org/10.1002/2013MS000269

Wing, A. A., Sobel, A. H., & Camargo, S. J. (2007). Relationship between the potential and actual intensities of tropical cyclones on interannual time scales. *Geophysical Research Letters*, *34*(8), 2006GL028. https://doi.org/10.1029/2006GL028581

Zhang, D.-L., & Chen, H. (2012). Importance of the upper-level warm core in the rapid intensification of a tropical cyclone. *Geophysical Research Letters*, *39*(2), 2011GL050. https://doi.org/10.1029/2011GL050578

References From the Supporting Information

Bretherton, C. S., Blossey, P. N., & Khairoutdinov, M. (2005). An energy-balance analysis of deep convective self-aggregation above uniform SST. *Journal of the Atmospheric Sciences*, *62*(12), 4273–4292. https://doi.org/10.1175/JAS3614.1

Collins, W. D., Rasch, P. J., Boville, B. A., Hack, J. J., McCaa, J. R., Williamson, D. L., et al. (2006). The formulation and atmospheric simulation of the community atmosphere model version 3 (CAM3). *Journal of Climate*, *19*(11), 2144–2161. https://doi.org/10.1175/JCLI3760.1